1 Formation and Structures of Silyl Radicals

1.1 METHODS OF GENERATION OF SILYL RADICALS

The reaction of atoms, radicals or excited triplet states of some molecules with silicon hydrides is the most important way for generating silyl radicals [1,2]. Indeed, Reaction (1.1) in solution has been used for different applications. Usually radicals X• are centred at carbon, nitrogen, oxygen, or sulfur atoms depending on the objective.

$$R_3SiH + X\bullet \longrightarrow R_3Si\bullet + XH \tag{1.1}$$

For example, photochemically produced *t*-BuO• radicals have been mainly used for the generation of silyl radicals to be studied by spectroscopic techniques (see Chapters 1 and 2). Carbon-centred X• radicals are of great importance in chemical transformations under reducing conditions, where an appropriate silane is either the reducing agent or the mediator for the formation of new bonds (see Chapters 4, 5 and 7). Chapter 3 is entirely dedicated to the hydrogen donor abilities of silicon hydrides towards a variety of radicals. In particular, a large number of available kinetic data are collected and analysed in terms of the substituent influence on the Si—H moiety and on the attacking radical.

Several methods for generating of silyl radicals exist using direct interaction of silanes with light (Reaction 1.2). However, none of them is of general applicability, being limited to some specific application [3].

$$R_3Si{-}Y \xrightarrow{h\nu} R_3Si\bullet + Y\bullet \tag{1.2}$$

The best example is the photochemistry of aryldisilanes, which undergo essentially three principal photoprocesses [4–6]. These include the silylene extru-

Organosilanes in Radical Chemistry C. Chatgilialoglu
 ISBN: 0-471-49870-X

sion, 1,3-Si shift to the *ortho* position of the aryl group to afford silatrienes and homolytic cleavage of Si—Si bond to give silyl radicals. Silenic products are derived from the lowest excited singlet state and are the major products in nonpolar solvents, while silyl radicals are derived from the lowest excited triplet state and are the major products in polar solvents such as acetonitrile [5]. The homolytic cleavage can also be promoted when the 1,3-Si migration is sterically hindered as shown in Reaction (1.3) [7]. Regarding the alkyl substituted oligo- and polysilanes, the silylene extrusion is the principal photoprocess in the far-UV photochemistry whereas reductive elimination of silylsilylene and homolytic Si—Si scission is also detected [8,9].

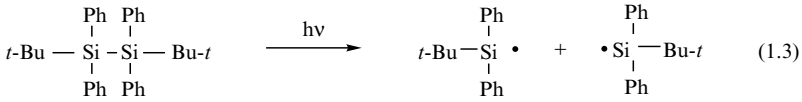

(1.3)

Organosiliconboranes having bulky substituents on the boron, e.g. $R_3SiB[N(CHMe)_2]_2$, exhibit UV absorption at wavelengths longer than 300 nm. Photolysis of this band afforded a pair of silyl and boryl radicals that can be trapped quantitatively by nitroxide (TEMPO) as shown in Reaction (1.4) [10].

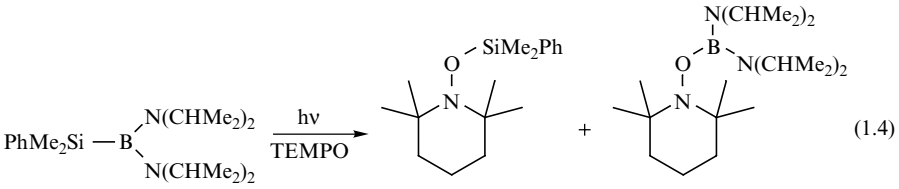

(1.4)

Silyl radicals have been produced by one-electron oxidation of silyl metals [11]. This is found to be the method of choice for the generation of persistent silyl radicals and allowed the preparation of the first isolable silyl radical (see later in this chapter). Reactions (1.5) and (1.6) show two sterically hindered silyl anions with Na^+ as the counter-cation, and their oxidation by the nitrosyl cation [12] and the complex $GeCl_2$/dioxane [13], respectively.

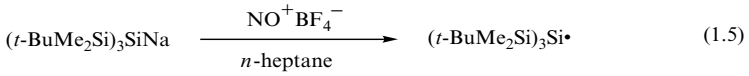

(1.5)

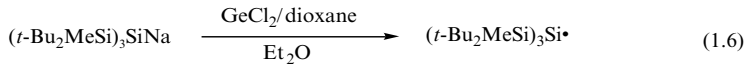

(1.6)

Silyl radicals are also involved as the reactive intermediates during one-electron reduction of bromosilanes. As an example, Reaction (1.7) shows the reduction by sodium of a silyl bromide to produce a persistent radical, which has been characterized by EPR spectroscopy [12].

$$(t\text{-BuMe}_2\text{Si})_3\text{SiBr} \xrightarrow[n\text{-heptane}]{\text{Na}} (t\text{-BuMe}_2\text{Si})_3\text{Si}\bullet \qquad (1.7)$$

Processes involving photoinduced electron transfer of organosilanes [3,14,15] have not been covered in this book with the exception of the following method that was successfully applied to various radical reactions, such as cyclizations, intermolecular additions and tandem annulations (see Chapters 4, 5 and 7). Silyl radicals have been obtained by a complex but efficient method using $PhSeSiR_3$ as the reagent. The strategy is based on the mesolysis of $PhSeSiR_3^{-\bullet}$ to give $R_3Si\bullet$ radical and $PhSe^-$ [16–18]. Indeed, the selective formation of $PhSeSiR_3^{-\bullet}$ is accomplished by visible-light irradiation (410 nm) of solutions containing $PhSeSiR_3$, 9,10-dimethoxyanthracene (DMA) as the electron donor, and ascorbic acid (H_2A) as the co-oxidant. Scheme 1.1 shows the photoinduced electron transfer with the formation of $PhSeSiR_3^{-\bullet}$ and $DMA^{+\bullet}$, together with the regeneration of DMA at the expense of ascorbic acid. The choice of the substituents is limited by their stabilities. Trialkyl substituted derivatives are highly sensitive to air and prone to hydrolysis, whereas the *t*-$BuPh_2Si$ derivative was found to be the most stable.

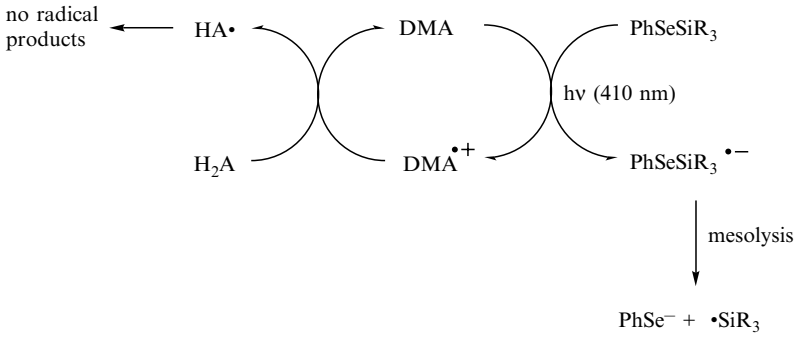

Scheme 1.1 Generation of silyl radicals by a photoinduced electron transfer method

$PhSeSiR_3$ reacts with Bu_3SnH under free radical conditions and affords the corresponding silicon hydride (Reaction 1.8) [19,20]. This method of generating $R_3Si\bullet$ radicals has been successfully applied to hydrosilylation of carbonyl groups, which is generally a sluggish reaction (see Chapter 5).

$$PhSeSiEt_3 + Bu_3SnH \xrightarrow[\text{benzene}]{\text{AIBN, 80 °C}} PhSeSnBu_3 + Et_3SiH \qquad (1.8)$$

Although a detailed mechanistic study is still lacking, it is reasonable to assume that the formation of $R_3Si\bullet$ radicals occurs by means of the mesolysis of reactive intermediate $PhSeSiR_3^{-\bullet}$, by analogy with the mechanistic information reported above. Indeed, an electron transfer between the initially

formed stannyl radical and the silyl selenide is more plausible (Reaction 1.9), than a bimolecular homolytic substitution at the seleno moiety.

$$PhSeSiEt_3 + Bu_3Sn\bullet \longrightarrow PhSeSiEt_3^{\bullet -} + Bu_3Si^{+} \qquad (1.9)$$

1.2 STRUCTURAL PROPERTIES OF SILYL RADICALS

Trisubstituted carbon-centred radicals chemically appear planar as depicted in the π-type structure **1**. However, spectroscopic studies have shown that planarity holds only for methyl, which has a very shallow well for inversion with a planar energy minimum, and for delocalized radical centres like allyl or benzyl. Ethyl, isopropyl, *tert*-butyl and all the like have double minima for inversion but the barrier is only about 300–500 cal, so that inversion is very fast even at low temperatures. Moreover, carbon-centred radicals with electronegative substituents like alkoxyl or fluorine reinforce the non-planarity, the effect being accumulative for multi-substitutions. This is ascribed to $n\sigma^*$ bonds between n electrons on the heteroatom and the bond to another substituent. The degree of bending is also increased by ring strain like in cyclopropyl and oxiranyl radicals, whereas the disubstituted carbon-centred species like vinyl or acyl are 'bent' σ radicals [21].

1

2

For a long time, this knowledge on carbon-centred radicals has driven the analysis of spectroscopic data obtained for silicon-centred (or silyl) radicals, often erroneously. The principal difference between carbon-centred and silyl radicals arises from the fact that the former can use only 2s and 2p atomic orbitals to accommodate the valence electrons, whereas silyl radicals can use 3s, 3p and 3d. The topic of this section deals mainly with the shape of silyl radicals, which are normally considered to be strongly bent out of the plane (σ-type structure **2**) [1]. In recent years, it has been shown that α-substituents have had a profound influence on the geometry of silyl radicals and the rationalization of the experimental data is not at all an extrapolation of the knowledge on alkyl radicals. Structural information may be deduced by using chemical, physical or theoretical methods. For better comprehension, this section is divided in subsections describing the results of these methods.

1.2.1 CHEMICAL STUDIES

The pyramidal structure of triorganosilyl radicals ($R_3Si\bullet$) was first indicated by chirality studies on optically active compounds containing asymmetric silicon.

For example, the α-naphthylphenylmethylsilyl radical (**3**) generated by hydrogen abstraction from the corresponding chiral silane reacts with CCl_4 to give optically active chlorosilane that has retained, at least in part, the configuration of the starting material [22]. Thus, the silyl radical is chiral and exists in a pyramidal form with considerable configurational stability, and it abstracts a chlorine atom from CCl_4 faster than its inversion (Reaction 1.10). Moreover, it was observed that the α-naphthylphenylmethylsilyl radical gave varying degrees of optical purity in the products as the concentration of CCl_4 was progressively diluted with benzene or cyclohexane. Analysis of these results by using a Stern–Volmer type of approach, yielded $k_{inv}/k = 1.30$ M at 80 °C, where k_{inv} is the rate constant for inversion at the silicon centre (Reaction 1.10) and k is the rate constant for the reaction of silyl radical with CCl_4 [23]. From these data, $k_{inv} = 6.8 \times 10^9\ s^{-1}$ at 80 °C is obtained which corresponds to an activation barrier of ca 23.4 kJ/mol if a normal preexponential factor of inversion is assumed, i.e., $\log(A/s^{-1}) = 13.3$. A number of other optically active organosilanes behave similarly, when the α-naphthyl group in α-NpSi*(Ph)(Me)H, is replaced by neo-C_5H_{11}, C_6F_5or Ph_2CH [22]. Under the same conditions, however, $Ph_3SiSi^*(Ph)(Me)H$ gave a chloride that was racemic indicating either that the inversion rate of the disilyl radical is much faster than its rate of reaction with CCl_4, or that the radical centre is planar.

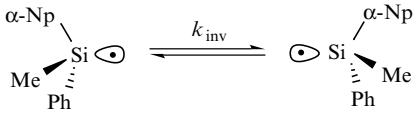

(1.10)

3

Analogous competitive kinetic studies have been reported for the inversion of silyl radicals **4** and **5** generated from corresponding silanes (Reaction 1.11) [24]. Rate constants for the interconversion of the two isomer radicals were estimated to be $k_1 \approx 9 \times 10^9\ s^{-1}$ and $k_{-1} \approx 4 \times 10^9\ s^{-1}$ at 0°C [23]. The equilibrium is slightly shifted to the right ($K \approx 2.3$) which suggests that radical **5** is a few hundred calories more stable than radical **4**. Activation energies for the forward and reverse inversion processes can be estimated to be ca 17–21 kJ/mol by assuming $\log(A/s^{-1}) = 13.3$.

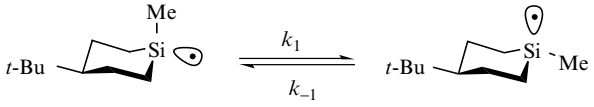

(1.11)

4 **5**

For comparison, it is worth mentioning that in the gas phase $H_3Si^\bullet$ is bent out of the plane by $(16.0 \pm 2.0)^\circ$, corresponding to an H—Si—H bond angle of $(112.5 \pm 2.0)^\circ$ and with an inversion barrier of 22.6 kJ/mol [25].

Structural information on silyl radicals has also been obtained from the isomerization of 9,10-dihydro-9,10-disilaanthracene derivatives **6** and **7** [26,27].

Indeed, irradiation of a pentane solution of either the *cis* isomer **6** or the corresponding *trans* isomer **7** in the presence of di-*tert*-butyl peroxide as radical initiator affords the same *cis*/*trans* mixture. For R = Me or Ph, a ratio of 47/53 is observed whereas for the more sterically hindered R = *t*-Bu a ratio of 81/19 is obtained. It was proposed that the radicals **9** and **10** generated by hydrogen abstraction from **6** and **7**, respectively, undergo inversion of the radical centre (Reaction 1.12) followed by hydrogen abstraction from the parent silanes (an identity reaction, see Chapter 3) [27]. Interestingly, the analogous 9-silaanthracene derivative **8** does not isomerize under identical conditions [8], suggesting that the disilaanthracene skeleton plays an important role either in lowering the activation energy of the identity reaction or fastening the inversion of silyl radical in Reaction (1.12).

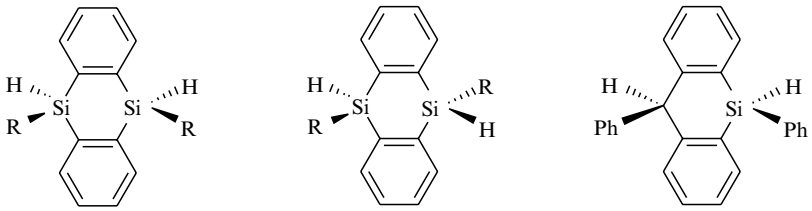

6 **7** **8**

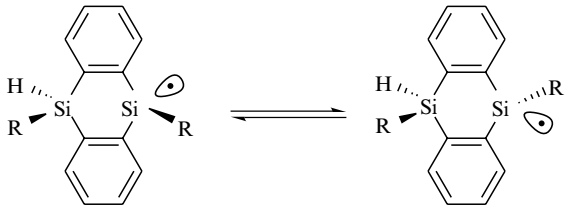

9 **10** (1.12)

1.2.2 ELECTRON PARAMAGNETIC RESONANCE (EPR) SPECTRA

EPR spectroscopy is the most important method for determining the structures of transient radicals. Information obtained from the EPR spectra of organic radicals in solution are: (i) the centre position of the spectra associated with *g* factors, (ii) the number and spacing of the spectral lines related to hyperfine splitting (hfs) constants, (iii) the total absorption intensity which corresponds to the radical concentration, and (iv) the line widths which can offer kinetic information such as rotational or conformational barriers. The basic principles as well as extensive treatments of EPR spectroscopy have been described in a number of books and reviews and the reader is referred to this literature for a general discussion [28–30].

Generally, the EPR spectra of silyl radicals show a central set of lines due to ^{1}H hfs constants and weaker satellites due to the coupling with $^{29}Si(I = 1/2, 4.7\ \%)$. The data for silyl radicals, presented in Table 1.1, have

Table 1.1 EPR data for a variety of α-substituted silyl radicals[a]

Silyl radical	$a(^{29}Si)$[b](G)	a(others) (G)	g factor
H_3Si•	189	7.96 (3 H)[c]	2.0032
H_2MeSi•	181	11.82 (2 H)[c]	2.0032
		7.98 (3 H)	
HMe_2Si•	183	16.99 (1 H)[c]	2.0031
		7.19 (6 H)	
Me_3Si•	181	6.28 (9 H)	2.0031
Et_3Si•	170	5.69 (6 H)	2.0030
		0.16 (9 H)	
t-Bu_3Si•	163	0.43 ($3^{13}C$)	
Ph_3Si•[d]	150		
Mes_3Si•[e]	135	0.70 (33 H)	2.0027
$(MeO)_3Si$•	339		2.0012
(t-$BuO)_3Si$•	331	0.23 (27 H)	2.0014
F_3Si•	498	136.6 (3 F)	2.0003
$MeCl_2Si$•	295	10.5 ($2^{35}Cl$)	2.0035
Cl_3Si•	416	12.4 ($3^{35}Cl$)	2.0035
$(Me_3Si)Me_2Si$•	137	8.21 (6 H)	2.0037
		0.47 (9 H)	
$(Me_3Si)_2MeSi$•	90	9.28 (3 H)	2.0045
		0.44 (18 H)	
$(Me_3Si)_3Si$•	64	7.1 ($3^{29}Si$)	2.0053
		0.43 (27 H)	

[a] See Reference [1] for the original citations.
[b] Because the magnetogyric ratio of ^{29}Si is negative, the signs of $a(^{29}Si)$ will also be negative.
[c] The sign is found to be positive by *ab initio* calculations [34].
[d] Phenyls are perdeuterated.
[e] Mes=2,4,6-trimethylphenyl.
Reprinted with permission from Reference [1]. Copyright 1995 American Chemical Society.

been chosen in order to include a variety of different substituents. In addition, isotropic hyperfine splitting and g factors are reported and most were obtained directly from solution spectra, although a few were taken from solid-state experiments. As an example, Figure 1.1 shows the EPR spectrum of $(Me_3Si)_2Si(•)Me$ radical obtained at $-40\,^{\circ}C$ by reaction of photogenerated t-BuO• radical with the parent silane [31]. The central quartet of relative intensity 1:3:3:1 with $a_H = 9.28\,G$ is caused by hyperfine coupling with the α-methyl protons. Each of these lines exhibits an additional hyperfine structure from 18 equivalent protons (six β-methyl groups) with $a_H = 0.44\,G$ (inset). The ^{29}Si-satellite regions were recorded with a 10-fold increase of the gain and are associated with $a(\alpha\text{-}^{29}Si) = 90.3\,G$.

Table 1.1 shows that the nature of the α-substituent in the radical centre enormously influences the ^{29}Si hfs constants. These constants, which can be used as a guide to the distribution of unpaired electron density, were initially correlated to changes in geometry at the radical centre by analogy with ^{13}C hfs constants of α-substituted alkyl radicals. Indeed, it was suggested that by

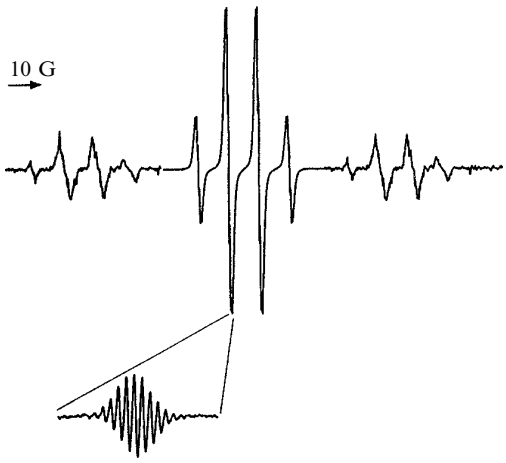

Figure 1.1 EPR spectrum of $(Me_3Si)_2Si(\bullet)Me$ recorded at 223 K. The satellite regions were recorded with a 10-fold increase of the gain. The inset shows an enlargement of the second spectral line recorded at lower modulation amplitude revealing hyperfine structure from 18 equivalent protons. Reprinted with permission from Reference [31]. Copyright 1992 American Chemical Society.

increasing the electronegativity of the α-substituents, the pyramidality of the silyl radical would increase, which would also mean a higher percentage of 3s character in the single occupied molecular orbital (SOMO), and therefore an increase in the ^{29}Si hfs, as well [32]. However, a theoretical study at the UMP2/DZP level reported that for a variety of α-substituted silyl radicals ($X_3Si\bullet$, where X = H, CH_3 NH_2, OH, F, SiH_3, PH_2, SH, Cl) the arrangement of atoms around silicon is essentially tetrahedral except for X = SiH_3 and that the large variation of the ^{29}Si hfs constants are due to the different distribution of the spin population at the Si center among 3s, 3p and 3d orbitals rather than to a change of geometry at the radical centre (see Section 1.2.5) [33,34]. The *g* factor of silyl radicals decreases along the series of substituents alkyl > alkoxyl > fluorine and silyl > chlorine (Table 1.1) while the spin–orbit coupling constant increases along the series C < O < F and Si < Cl [28]. Generally the *g* factor is larger than the free electron value of 2.00229 if spin–orbit coupling mixes the SOMO with low lying LUMOs and smaller if the mixing is with high lying doubly occupied orbitals. Moreover, the extent of the odd electron delocalization onto the atoms or groups attached to silicon is also expected to have an important influence on the *g* factor trend. Another factor affecting the magnitude of the *g* value is the geometry of the radical centre. Readers should refer to a general text on EPR for a more detailed discussion on the interpretation of hfs constants and *g* factors [29,30].

α-Aryl-substituted silyl radicals have been a subject of attraction in order to evaluate the extent to which a silicon centre radical can conjugate with an adjacent aromatic system. However, the high reactivity of the silyl radical

towards aromatic substitution (see Section 5.1.1), limited the detection of this type of transients by EPR spectroscopy. For example, $PhH_2Si\bullet$, $Ph_2HSi\bullet$ and $Ph_3Si\bullet$ radicals have not been observed in solution whereas the corresponding perdeuterated silyl radicals have been detected in a solid matrix [35]. Two sterically hindered analogous radicals, trimesitylsilyl and tris(3,5-di-*tert*-butylphenyl)silyl have been observed by EPR in solution and appear to be partially delocalized species according to the ring proton hfs constants [36,37]. Similar considerations and analogous experiments have been extended to α-vinyl substituted silyl radicals and the results are in line with the α-phenyl substituted case [38]. The spectra of Me_3Si-substituted silyl radicals are of particular interest. Thus, when Me_3Si groups progressively replace methyl groups, the ^{29}Si hfs constants decrease from 181 G in the $Me_3Si\bullet$ radical to 64 G in the $(Me_3Si)_3Si\bullet$ radical (Table 1.1). This trend is due mainly to the spin delocalization onto the Si—C β-bond and in part to the decrease in the degree of pyramidalization at the radical centre caused by the electron-releasing Me_3Si group [39].

Kinetic information from the line width alterations of EPR spectra by changing the temperature has been obtained for a number of silacycloalkyl radicals [40,41]. For example, silacyclopentyl radical exists at low temperature (−119 °C) in two equivalent twist conformations (**11** and **12**), which interconvert at higher temperature (15 °C). The Arrhenius parameters for such interconversion are $\log A/s^{-1} = 12.0$ and $E_a = 21.3\,kJ/mol$.

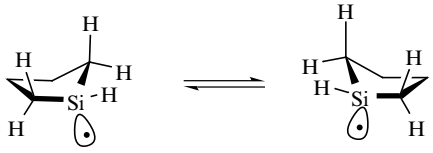

(1.13)

11 **12**

Persistent and stable silyl radicals have attracted considerable attention [42]. Bulky aryl or alkyl groups that generally make carbon-centred radicals persistent [43,44] have a much weaker effect on the silyl radicals. The high reactivity of the $Ph_3Si\bullet$ radical contrary to the stable $Ph_3C\bullet$ radical is mentioned above. The decay of the trimesitylsilyl radical at −63°C follows a first-order kinetics with a half-life of 20 s [37]. Tri-*tert*-butylsilyl radical is also not markedly persistent showing the modest tendency of *tert*-butyl groups to decrease pyramidalization [45]. The most persistent trialkyl-substituted silyl radical is $[(Me_3Si)_2CH]_3Si\bullet$, which at 20 °C follows a first-order decay with a half-life of 480 s [36]. An exceptionally stable diradical was isolated by reaction of 1,1-dilithio-2,3,4,5-tetraphenylsilole with 1,1-dichloro-2,3-diphenylcyclopropene, for which the structure **13** was suggested on the basis of EPR data and theoretical calculations [46]. The remarkable unreactivity of this diradical has been explained by steric hindrance, as well as delocalization of the unpaired electrons over the silole ring.

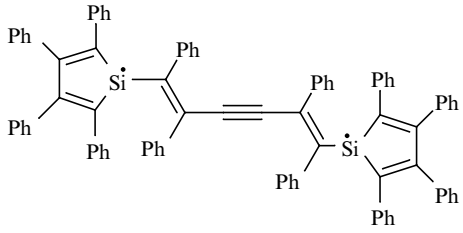

13

On the other hand, bulky trialkylsilyl substituents have a profound effect on the structure of silyl radicals. Indeed, by increasing the steric effect with more crowded trialkylsilyl substituents the persistency of silyl radicals increases substantially. Table 1.2 reports the EPR data for a variety of tris(trialkylsilyl)silyl radicals in comparison with the prototype $(Me_3Si)_3Si\bullet$. Inspection of the data shows the α-^{29}Si hfs constants tend to decrease and the β-^{29}Si hfs slightly increase when the methyl group is progressively replaced by a bulkier group, the effect being cumulative, e.g., along the series $(Me_3Si)_3Si\bullet$, $(Et_3Si)_3Si\bullet$, $(i-Pr_3Si)_3Si\bullet$ and $(Me_3Si)_3Si\bullet$, $(Et_2MeSi)_3Si\bullet$, $(t\text{-}Bu_2MeSi)_3Si\bullet$. These trends have been associated with an increase of the polysilane skeleton flattening through the series [12,13,48–50]. Indeed, the half-lives of the radicals increase within the series and the $(t\text{-}Bu_2MeSi)_3Si\bullet$ radical is found to be stable and isolable in a crystal form. Therefore, the radicals $(Et_3Si)_3Si\bullet$, $(i\text{-}Pr_3Si)_3Si\bullet$, $(t\text{-}BuMe_2Si)_3Si\bullet$ and $(t\text{-}Bu_2MeSi)_3Si\bullet$ have a practically planar structure due to the steric repulsions among the bulky silyl substituents. The small differences of their α-^{29}Si hfs constants are presumably due to different degrees of spin delocalization onto the Si—C β-bond, as a consequence of conformational effects in order to minimize the steric hindrance. Persistent silyl radicals have also been formed upon

Table 1.2 EPR data for a variety of tris(trialkylsilyl)silyl radicals

Silyl radical	$a(\alpha$-^{29}Si)(G)	$a(\beta$-^{29}Si)(G)	a(others) (G)	g factor	Reference
$(Me_3Si)_3Si\bullet$	63.8	7.1	0.43 (27 H)	2.0053	[47]
$(EtMe_2Si)_3Si\bullet$	62.8	7.1	0.37 (18 H) 0.14 (6 H)	2.0060	[48]
$(Et_2MeSi)_3Si\bullet$	60.3	7.3	0.27 (12 H) 0.15 (9 H) 3.2 ($3\,^{13}$C)	2.0060	[48]
$(Et_3Si)_3Si\bullet$	57.2	7.9	0.12 (18 H) 3.0 ($3\,^{13}$C)	2.0063	[48]
$(i\text{-}Pr_3Si)_3Si\bullet$	55.6	8.1	2.2 ($3\,^{13}$C)	2.0061	[49]
$(t\text{-}BuMe_2Si)_3Si\bullet$	57.1	8.1	0.33 (27 H) 0.11 (18 H)	2.0055	[12]
$(Me_3SiMe_2Si)_3Si\bullet$	59.9	7.4		2.0065	[50]
$(t\text{-}Bu_2MeSi)_3Si\bullet$	58.0	7.9		2.0056	[13]

photolysis of poly(di-*n*-alkylsilanes) in solution via a complex reaction mechanism [8]. Radical **14** (Hx = *n*-hexyl) with $g = 2.0047$, $a(\alpha\text{-}^{29}\text{Si}) = 75\,\text{G}$ and $a(\beta\text{-}^{29}\text{Si}) = 5.8\,\text{G}$, showed line-broadening effects as the temperature was lowered. This observation has been correlated to the restricted rotational motion about the C—Si• bond and, in particular, to a rocking interchange of the two α-hydrogens. Isolation of 'allylic-type' silyl radical **15** has also been achieved [51]. The EPR spectrum consists of a broad singlet ($g = 2.0058$) with three doublet satellite signals due to coupling with ^{29}Si of 40.7, 37.4 and 15.5 G. The two doublets with 40.7 and 37.4 G broaden upon raising the temperature and coalesce at 97 °C due to the rotation of the *t*-BuMe$_2$Si group. The magnitude of ^{29}Si hfs constants is consistent with the delocalization of the unpaired electron over the three silicon atoms in the ring, but it is noteworthy that the coupling constants of the outer Si atoms are not equal. This is explained below.

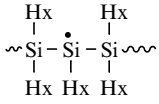

14

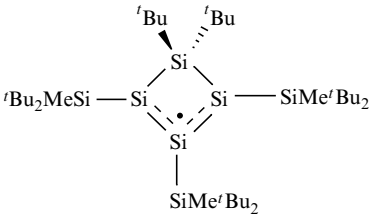

15

1.2.3 CRYSTAL STRUCTURES

The crystal structures of two isolable silyl radicals have recently been reported. The bulky substituted (*t*-Bu$_2$MeSi)$_3$Si• radical was isolated as air-sensitive yellow needles [13], whereas the conjugated and bulky substituted cyclotetrasilenyl radical **15** was obtained as red–purple crystals [51].

Figure 1.2 shows a completely planar geometry around the Si1 atom of (*t*-Bu$_2$MeSi)$_3$Si• radical. Indeed, the bond angles Si2—Si1—Si3, Si2—Si1—Si4 and Si3—Si1—Si4 are 119.49°, 120.08° and 120.43°, respectively, their sum being exactly 360°. The Si—Si bonds are larger (2.42 ± 0.01 Å) than normal. Interestingly, all the methyl substituents at the α-Si atoms (i.e., C1, C4 and C7) are located in the plane of the polysilane skeleton in order to minimize steric hindrance. As reported in the previous section, the planarity of this radical is retained in solution.

Figure 1.3 shows the ORTEP drawing of the conjugated radical **15**. The four-membered ring is nearly planar with the dihedral angle between the radical part Si1—Si2—Si3 and Si1—Si4—Si3 being 4.7°. The Si1 and Si2 atoms have planar geometry (the sums of the bond angles around them are 360.0° and 359.1°, respectively) whereas the Si3 atom is slightly bent (356.2°). This small asymmetry of the moiety where the radical is delocalized is also observed in the

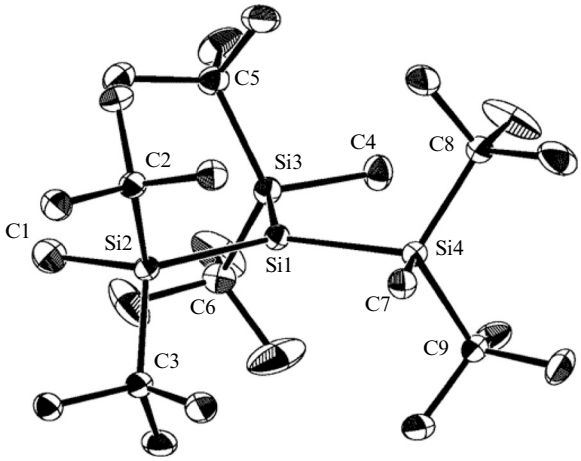

Figure 1.2 Molecular structure of $(t\text{-Bu}_2\text{MeSi})_3\text{Si}\bullet$ radical with thermal ellipsoids drawn at the 30% level (hydrogen atoms are omitted for clarity). Reprinted with permission from Reference [13]. Copyright 2002 American Chemical Society.

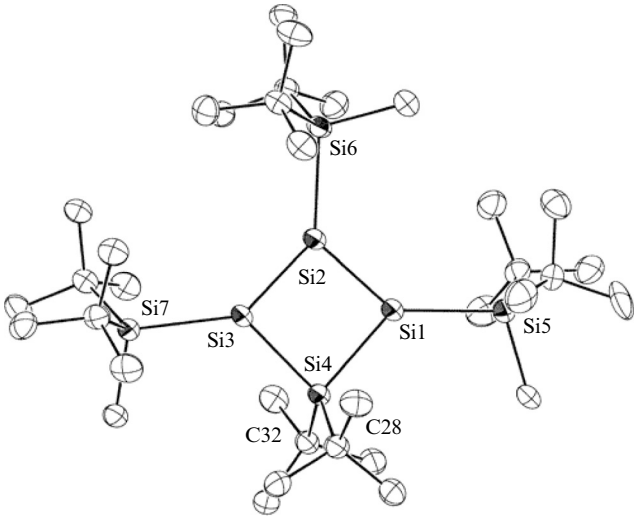

Figure 1.3 ORTEP Drawing of cyclotetrasilenyl radical **15**. Hydrogen atoms are omitted for clarity. Reprinted with permission from Reference [51]. Copyright 2001 American Chemical Society.

Si—Si bond length, the Si1—Si2 being slightly shorter than Si2—Si3 (2.226 vs 2.263 Å), and explains the magnetic inequivalence of Si1 and Si3 noted above.

The reaction of $(t\text{-Bu}_2\text{MeSi})_3\text{Si}\bullet$ radical with lithium in hexane at room temperature afforded the silyllithium **16** for which the crystal structure shows

the central anionic silicon atom to be almost planar (119.7° for Si—Si—Si bond angles) and the Si—Si bond lengths significantly shorter (2.36 Å) than in the radical (2.42 Å) [52]. Similarly, the cyclotetrasilenyl radical **15** reacted with lithium to give the corresponding lithiated derivative, which has a π-type structure with coordination of a lithium cation to a trisilaallyl moiety [53]. It is also worth mentioning that the crystal structure of $[(i\text{-Pr})_3Si]_3SiH$ shows a nearly planar structure of the polysilane skeleton [49]. In fact, the Si—Si—Si bond angles are 118.1° and the sum of the three angles around the central silicon atom is 354.3°. The Si—Si—H bond angle is 98.0°. Therefore, the introduction of bulky silyl groups induces a significant flattening of the silicon skeleton by large steric repulsion even in silicon hydride. Such steric hindrances should play an even more important role in the planarization of the corresponding silyl radicals.

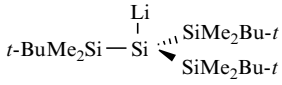

16

1.2.4 UV–VISIBLE SPECTRA

The electronic absorption spectra of few trialkylsilyl radicals have been recorded in both gas and liquid phases. Radicals $R_3Si\bullet$ (R = Me, Et, *n*-Pr) generated in the gas phase exhibit a strong band in the region of 220–300 nm with a maximum at ca 260 nm ($\varepsilon_{max} = 7500\ M^{-1}\ cm^{-1}$ for $Me_3Si\bullet$) [54,55]. Figure 1.4 shows the UV–visible spectrum of $Et_3Si\bullet$ in liquid isooctane, which exhibits a continuously increasing absorption below 340 nm, with no maximum above 280 nm ($\varepsilon_{308} = 1100\ M^{-1}\ cm^{-1}$), and a weak symmetric band between 350 and 450 nm, with a maximum at 390 nm [56].

The transient absorption spectra of silyl radicals with the Me group of $Me_3Si\bullet$ progressively replaced by Ph or Me_3Si groups were also studied. $PhMe_2Si\bullet$, $Ph_2MeSi\bullet$, and $Ph_3Si\bullet$ exhibit a strong band in the range of 290–360 nm attributed to the electronic transition involving the aromatic rings and a weak absorption between 360 and 550 nm (see Figure 1.4 for $Ph_3Si\bullet$) [56]. In the series of Me_3Si-substituted silyl radicals, $Me_3SiSi(\bullet)Me_2$ exhibits a band between 280 and 450 nm with a maximum at ca 310 nm and a shoulder at longer wavelengths [57], whereas the spectrum of $(Me_3Si)_3Si\bullet$ radical shows a continuously increasing absorption below ca 350 nm and no maximum above 280 nm [47].

The absorption spectra of the $(RS)_3Si\bullet$ radicals (R = Me, *i*-Pr) exhibit a strong band at 300–310 nm. In addition, the absorption envelopes extend well out into the visible region of the spectrum to about 500 nm and show a shoulder at ca 425 nm (see Figure 1.4 for $(MeS)_3Si\bullet$) [58].

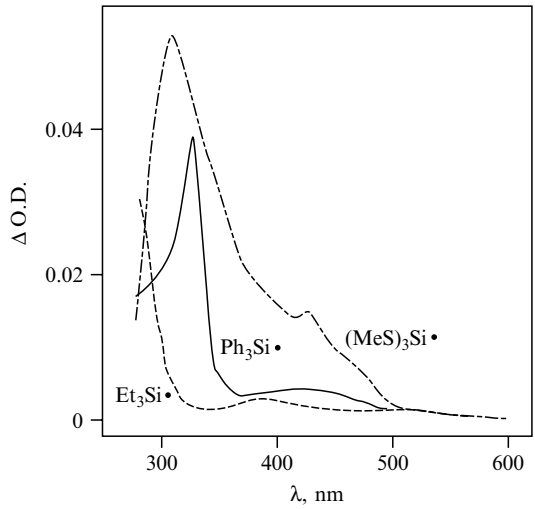

Figure 1.4 Transient spectra for some R_3Si• radicals generated by reaction of *t*-BuO• with the corresponding silanes under similar experimental conditions. Reprinted in part with permission from Reference [56]. Copyright 1983 American Chemical Society.

1.2.5 THEORETICAL STUDIES

There has been a number of theoretical studies on a variety of silyl radicals at various levels of *ab initio* theory. The structural parameters for a variety of halogenated silyl radicals, i.e., $F_{3-n}Si(\bullet)H_n$, $Cl_{3-n}Si(\bullet)H_n$, and $Cl_{3-n}Si(\bullet)F_n$, (with n having values from 0 to 3) have been examined with the 6-31 ++ G* basis set, with optimization at the UHF level and single point calculations at the UMP2 level [59]. All radicals have bond angles close to the ideal tetrahedral angle. Both vertex inversion (transition state **17**) and edge inversion (transition state **18**) mechanisms were taken into consideration. For the H_3Si• radical, the calculated barriers for the **17** and **18** transition states are 20.5 and 277.4 kJ/mol, respectively. Similarly, FH_2Si•, ClH_2Si• and Cl_2HSi• all invert by the vertex mechanism. However, for the F_2HSi• radical the calculated barriers for the two mechanisms are almost identical, and increased halogenation results in a change of mechanism. Thus all $Cl_{3-n}Si(\bullet)F_n$ radicals invert by the edge mechanism.

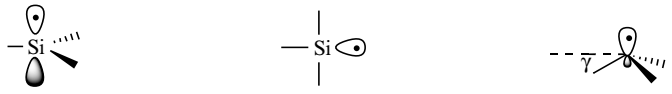

17 **18** **19**

The optimized structural parameters of the α-trisubstituted silyl radical (X_3Si•, where X = H, CH_3, NH_2OH, F, SiH_3, PH_2, SH and Cl) were performed at the UMP2/DZP level of theory [33]. As expected, the bond lengths decrease

according to electronegativity. The calculated angles γ (see structure **19**) for the silyl radicals with different substituents (in parentheses) are: 17.73° (H), 18.69° (CH_3), 21.53° (NH_2), 20.76° (OH), 20.77° (F), 13.40° (SiH_3), 22.68° (PH_2), 20.51° (SH), and 19.43° (Cl). Therefore, for all these trisubstituted radicals, the arrangement of atoms around the silicon is found to be essentially tetrahedral with the exception of the $(H_3Si)_3Si•$ radical which is much less bent. The magnitude and the trend of the ^{29}Si hfs constants from EPR spectra are well reproduced by these calculations and are due to more 3s character of the unpaired electron orbital at the Si-center rather than to a general change of geometry at radical centre. The calculations show that in the SOMO the delocalization of the unpaired electron onto the α-substituent increases from second to third row elements, whereas the population on Si-3s increases linearly with the increasing electronegativity of the α-substituent. For example, the calculated distribution of the unpaired electron density for $Me_3Si•$ is 81% on silicon (14.3% in 3s, 64.6% in 3p, and 2.1% in 3d) and 19% on methyls; for $F_3Si•$ it is 84.4% on silicon (41.8% in 3s, 32.6% in 3p, and 6.4% in 3d) and 15.6% on fluorines; for $Cl_3Si•$ it is 57.3% on silicon (21.5% in 3s, 32.6% in 3p, and 3.2% in 3d) and 42.7% on chlorines. UMP2/DZP/TZP calculations have been extended to the series $H_{3-n}Si(•)Me_n$($n = 0$–2) addressing the early controversy about the signs of α-^1H hfs constants [34]. The sign was found to be positive for all these radicals, which have a nearly tetrahedral geometry at silicon. The same level of theory has been used to calculate the α-^{29}Si hfs constants of series $Me_{3-n}Si(•)Cl_n$ and $Me_{3-n}Si(•)(SiMe_3)_n$($n = 0$–3) and to analyse observed trends [60]. The large increase of the ^{29}Si hfs when Me is successively replaced by Cl is mainly due to the change of the Si orbital populations rather than to structural changes, whereas when Me is replaced by $SiMe_3$ the considerable decrease is due to the increased spin delocalization and the flatter geometry.

The structural parameters of $(HS)_3Si•$ radicals were computed at the HF/6-31G* level for C_3 symmetry [58]. The radical centre at silicon is pyramidal. Two minima have been found along the energy surface generated by the synchronous rotation of the SH groups. In the most stable conformation **20**, the hydrogens adopt a gauche conformation ($\omega = 50°$) with respect to the SOMO, which is mainly the sp_3 atomic orbital (AO) of Si. In the other minimum **21**, which is 18.4 kJ/mol higher in energy, the hydrogens are nearly anti ($\omega = 150°$) with respect to the SOMO.

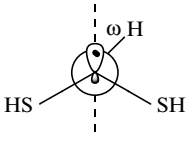

20

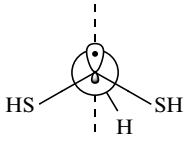

21

Multiple scattering Xα (MSXα) method was applied to assign the optical absorption spectra of $Me_3Si•$ and $(MeS)_3Si•$ radicals. The strong band

observed for $(alkyl)_3Si•$ radicals at ca 260 nm has been attributed to the superimposition of the valence transition from the MO localized at the Si—C bond to the SOMO and of the transition from the SOMO to the 4p Rydberg orbital [61]. Furthermore the observed weak band between 350 and 450 nm for $Et_3Si•$ radical (Figure 1.4) has been assigned to the transition from SOMO to the 4s Rydberg orbital. For the $(MeS)_3Si•$ radical [58], the strong band has been attributed to transitions from the SOMO (localized mainly at the 3p AO of Si) to the antibonding σ^*_{Si-S}MOs (a_1 and e symmetry). A contribution to the intensity of this band could also derive from the valence transition from the $\sigma_{Si-S}(a_1)$ MO to the SOMO and from the Rydberg transition from the SOMO to the $4p(a_1)$ orbital. The weak band/shoulder at ca 425 nm has been assigned to the valence excitation from the MO localized at the Si—S bond to the SOMO. Transitions from sulfur lone pairs to the SOMO have much lower oscillator strengths and are predicted to occur in the near-infrared region.

1.3 REFERENCES

1. Chatgilialoglu, C., *Chem. Rev.*, 1995, **95**, 1229.
2. Chatgilialoglu, C., and Newcomb, M., *Adv. Organomet. Chem.*, 1999, **44**, 67.
3. Steinmetz, M.G., *Chem. Rev.*, 1995, **95**, 1527.
4. Leigh, W.J., and Sluggett, G.W., *J. Am. Chem. Soc.*, 1993, **115**, 7531.
5. Leigh, W.J., and Sluggett, G.W., *Organometallics*, 1994, **13**, 269.
6. Sluggett, G.W., and Leigh, W.J., *Organometallics*, 1994, **13**, 1005.
7. Sluggett, G.W., and Leigh, W.J., *Organometallics*, 1992, **11**, 3731.
8. McKinley, A.J., Karatsu, T., Wallraff, G.M., Thompson, D.P., Miller, R.D., and Michl, J., *J. Am. Chem. Soc.*, 1991, **113**, 2003.
9. Davidson, I.M.T., Michl, J., and Simpson, T., *Organometallics*, 1991, **10**, 842.
10. Matsumoto, A., and Ito, Y., *J. Org. Chem.*, 2000, **65**, 5707.
11. Tamao, K., and Kawachi, A., *Adv. Organomet. Chem.*, 1995, **38**, 1.
12. Kira, M., Obata, T., Kon, I., Hashimoto, H., Ichinohe, M., Sakurai, H., Kyushin, S., and Matsumoto, H., *Chem Lett.*, 1998, 1097.
13. Sekiguchi, A., Fukawa, T., Nakamoto, M., Lee, V. Ya., and Ichinohe, M., *J. Am. Chem. Soc.*, 2002, **124**, 9865.
14. Shizuka, H., and Hiratsuka, H., *Res. Chem. Intermed.*, 1992, **18**, 131.
15. Kako, M., and Nakadaira, Y., *Coord. Chem. Rev.*, 1998, **176**, 87.
16. Pandey, G., and Rao, K.S.S.P., *Angew. Chem. Int. Ed. Engl.*, 1995, **34**, 2669.
17. Pandey, G., Rao, K.S.S.P., Palit, D.K., and Mittal, J.P., *J. Org. Chem.*, 1998, **63**, 3968.
18. Pandey, G., Rao, K.S.S.P., and Rao, K.V.N., *J. Org. Chem.*, 2000, **65**, 4309.
19. Nishiyama, Y., Kajimoto, H., Kotani, K., and Sonoda, N., *Org. Lett.*, 2001, **3**, 3087.
20. Nishiyama, Y., Kajimoto, H., Kotani, K., Nishida, T., and Sonoda, N., *J. Org. Chem.*, 2002, **67**, 5696.
21. Symons, M.C.R., *Chemical and Biochemical Aspects of Electron-Spin Resonance Spectroscopy*, Van Nostrand Reinhold, Melbourne, 1978.
22. Sommer, L.H., and Ulland, L.A., *J. Org. Chem.*, 1972, **37**, 3878.
23. Chatgilialoglu, C., Ingold, K.U., and Scaiano, J.C., *J. Am. Chem. Soc.*, 1982, **104**, 5123.
24. Sakurai, H., and Murakami, M., *Bull. Chem. Soc. Jpn.*, 1977, **50**, 3384.

25. Nimlos, M.R., and Ellison, G.B., *J. Am. Chem. Soc*., 1986, **108**, 6522.
26. Kyushin, S., Shinnai, T., Kubota, T., and Matsumoto, H., *Organometallics*, 1997, **16**, 3800.
27. Nishiyama, K., Oba, M., Takagi, H., Saito, T., Imai, Y., Motoyama, I., Ikuta, S., and Hiratsuka, H., *J. Organomet. Chem*., 2001, **626**, 32.
28. Fischer, H. In *Free Radicals*, Vol. II, J.K. Kochi (Ed.), Wiley, New York, 1973, p. 435.
29. Atherton, N.M., *Principles of Electron Spin Resonance*, Ellis Horwood, Chichester, 1993.
30. Weil, J.A., Bolton, J.R., and Wertz, J.E., *Electron Paramagnetic Resonance: Elementary Theory and Practical Applications*, Wiley, New York, 1994.
31. Chatgilialoglu, C., Guerrini, A., and Lucarini, M., *J. Org. Chem*., 1992, **57**, 3405.
32. Alberti, A., and Pedulli, G.F., *Rev. Chem. Intermed*., 1987, **8**, 207.
33. Guerra, M., *J. Am. Chem. Soc*., 1993, **115**, 11926.
34. Guerra, M., *Chem. Phys. Lett*., 1995, **246**, 251.
35. Lim, W-L., and Rhodes, C.J., *J. Chem. Soc., Chem. Commun*., 1991, 1228.
36. Gynane, M.J.S., Lappert, M.F., Riley, P.I., Rivière, P., and Rivière-Baudet, M., *J. Organomet. Chem*., 1980, **202**, 5.
37. Sakurai, H., Umino, K., and Sagiyama, H., *J. Am. Chem. Soc*., 1980, **102**, 6837.
38. Jackson, R.A., and Zarkadis, A.K., *Tetrahedron Lett*., 1988, **29**, 3493.
39. Guerra, M., *J. Chem. Soc., Perkin Trans. 2*, 1995, 1817.
40. Jackson, R.A., and Zarkadis, A.K., *J. Chem. Soc., Perkin Trans. 2*, 1990, 1139.
41. Jackson, R.A., and Zarkadis, A.K., *J. Chem. Soc., Faraday Trans*., 1990, **86**, 3229.
42. Power, P.P., *Chem. Rev*., 2003, **103**, 789.
43. Griller, D., and Ingold, K.U., *Acc. Chem. Res*., 1976, **8**, 13.
44. Griller, D., and Ingold, K.U., *Acc. Chem. Res*., 1980, **13**, 193.
45. Jackson, R.A., and Weston, H., *J. Organomet. Chem*., 1984, **277**, 13.
46. Toulokhonova, I.S., Stringfellow, T.C., Ivanov, S.A., Masunov, A., and West, R., *J. Am. Chem. Soc*., 2003, **125**, 5767.
47. Chatgilialoglu, C., and Rossini, S., *Bull. Soc. Chim. Fr*., 1988, 298.
48. Kyushin, S., Sakurai, H., Betsuyaku, T., and Matsumoto, H., *Organometallics*, 1997, **16**, 5386.
49. Kyushin, S., Sakurai, H., and Matsumoto, H., *Chem. Lett*., 1998, 107.
50. Apeloig, Y., Bravo-Zhivotovskii, D., Yuzefovich, M., Bendikov, M., and Shames, A.I., *Appl. Magn.Reson*., 2000, **18**, 425.
51. Sekiguchi, A., Matsuno, T., and Ichinohe M., *J. Am. Chem. Soc*., 2001, **123**, 12436.
52. Nakamoto, M., Fukawa, T., Lee, V. Ya., and Sekiguchi, A., *J. Am. Chem. Soc*., 2002, **124**, 15160.
53. Matsuno, T., Ichinohe M., and Sekiguchi, A., *Angew. Chem. Int. Ed*., 2002, **41**, 1575.
54. Shimo, N., Nakashima, N., and Yoshihara, K., *Chem. Phys. Lett*., 1986, **125**, 303.
55. Brix, Th., Paul, U., Potzinger, P., and Reimann, B., *J. Photochem. Photobiol., A: Chem*., 1990, **54**, 19.
56. Chatgilialoglu, C., Ingold, K.U., Lusztyk, J., Nazran, A.S., and Scaiano, J.C., *Organometallics,* 1983, **2**, 1332.
57. Lusztyk, J., Maillard, B., and Ingold, K.U., *J. Org. Chem*., 1986, **51**, 2457.
58. Chatgilialoglu, C., Guerra, M., Guerrini, A., Seconi, G., Clark, K.B., Griller, D., Kanabus-Kaminska, J., and Martinho-Simões, J. A., *J. Org. Chem*., 1992, **57**, 2427.
59. Hopkinson, A.C., Rodriquez, C.F., and Lien, M.H., *Can. J. Chem*., 1990, **68**, 1309.
60. Guerra, M., *J. Chem. Soc., Perkin Trans. 2*, 1995, 1817.
61. Chatgilialoglu, C., and Guerra, M., *J. Am. Chem. Soc*., 1990, **112**, 2854.